PROCEEDINGS OF SCIENCE

Combined fit to the spectrum and composition data measured by the Pierre Auger Observatory including magnetic horizon effects

Juan Manuel González[a,*] **for the Pierre Auger Collaboration**[b]

[a] *CONICET, Centro Atomico Bariloche, Argentina.*

[b] *Observatorio Pierre Auger, Av. San Martín Norte 304, 5613 Malargüe, Argentina*
Full author list: https://www.auger.org/archive/authors_icrc_2023.html

E-mail: spokespersons@auger.org

The measurements by the Pierre Auger Observatory of the energy spectrum and mass composition of cosmic rays can be interpreted assuming the presence of two extragalactic source populations, one dominating the flux at energies above a few EeV and the other below. To fit the data ignoring magnetic field effects, the high-energy population needs to accelerate a mixture of nuclei with very hard spectra, at odds with the approximate E^{-2} shape expected from diffusive shock acceleration. The presence of turbulent extragalactic magnetic fields in the region between the closest sources and the Earth can significantly modify the observed CR spectrum with respect to that emitted by the sources, reducing the flux of low-rigidity particles that reach the Earth. We here take into account this magnetic horizon effect in the combined fit of the spectrum and shower depth distributions, exploring the possibility that a spectrum for the high-energy population sources with a shape closer to E^{-2} be able to explain the observations. We find that a large inter-source separation d_s and a large magnetic field RMS amplitude within the Local Supercluster region, such that $B_{\rm rms} \simeq 100\,{\rm nG}\,(40\,{\rm Mpc}/d_{\rm s})\sqrt{25\,{\rm kpc}/L_{\rm coh}}$, are needed to interpret the data within this scenario, where $L_{\rm coh}$ is the magnetic field coherence length.

38th International Cosmic Ray Conference (ICRC2023)
26 July - 3 August, 2023
Nagoya, Japan

[*] Juan Manuel González

PoS(ICRC2023)288

1. Introduction

The cosmic ray (CR) flux and depth of shower maximum ($X_{\max}$) distributions measured by the Pierre Auger Observatory have been used to constrain the properties of the CR sources [1–3]. In order to explain the observations above $10^{17.8}$ eV two different source populations are required. The first population, referred to as the low-energy component (L), dominates the flux below few EeV. The second population, referred to as the high-energy component (H), dominates the flux at higher energies. Considering that these populations consist of continuously distributed equally luminous sources with the different mass components having power-law spectra with rigidity dependent cutoffs, a maximum likelihood fit leads to a spectrum for the high-energy component much harder than the expectations from diffusive shock acceleration. In the presence of intergalactic magnetic fields and taking into account the finite inter-source distances, one expects however a depletion of the flux of low-energy particles for which the diffusion time from the closest sources becomes larger than the age of the sources. This effect would modify the spectrum of the particles reaching the Earth and hence affect the inferred source spectrum.[1] We analyse the magnetic field and cosmic ray source parameters for which this effect is relevant if one wishes to account for the observations.

1.1 Astrophysical model

The CR source populations ($x = L$ or H) are modelled considering a rate of emission per unit of volume, time and energy for particles with mass A, energy E and charge Z, given by

$$\dot{Q}_{A,x}(z,E) = \dot{Q}_{0,x}\xi_x(z) f_{A,x} \times \left(\frac{E}{E_0}\right)^{-\gamma_x} F_{\rm cut}\left(\frac{E}{ZR^x_{\rm cut}}\right). \tag{1}$$

The normalisation $\dot{Q}_{0,x}$ is the present total differential rate of CR emission at the reference energy E_0 (much smaller than the hydrogen cutoff $R^x_{\rm cut}$), at which the relative source fractions of the different elements with mass number A are $f_{A,x}$. We consider that the sources emit the representative elements H, He, N, Si and Fe. The function ξ_x takes into account the evolution in redshift z of the emissivity. We will consider two cases: the no evolution (NE) scenario with $\xi = 1$ up to $z = 1$, and that of emissivities scaling with the star formation rate (SFR) as parameterised in [5], so that $\xi \propto (1+z)^{3.44}$ up to $z = 0.97$ and then decays as $\xi \propto (1+z)^{-0.26}$, and we consider in this case $z < 4$. The function $F_{\rm cut}$ provides a rigidity cutoff that suppresses the flux above an energy $ZR^x_{\rm cut}$. We will assume for it an hyperbolic secant shape, with $F_{\rm cut}(x) = {\rm sech}(x^\Delta)$, where Δ determines the steepness of the cutoff and we will explore values of Δ equal to 1, 2 or 3.

The particles emitted at the sources are propagated until they reach the Earth using the SimProp software [6]. The resulting fluxes depend on the nuclear photo-disintegration cross sections as well as on the extragalactic background light model considered to evaluate the interactions during propagation. We adopt in the analysis the photodisintegration cross section from TALYS [7] and the extragalactic background radiation from Gilmore et al. [8]. The inferred composition depends on the hadronic interactions model used to interpret the $X_{\max}$ measurements, which was found in [1, 3] to be the assumption that mostly affected the conclusions. We will explore the dependence of the results on the hadronic interaction models by considering both EPOS-LHC [9] and Sibyll 2.3d [10].

[1] CR interactions at the source may also change the emitted spectrum with respect to the accelerated one [4].

The nuclei reaching Earth will be grouped by mass number as $A = 1$ (H), 2–4 (He), 5–16 (N), 17–30 (Si) and 31-56 (Fe). Nuclei reaching us as part of the same mass group in which they were produced will be referred to as *primary nuclei*. Nuclei produced via photo-disintegration arriving at Earth as part of a different mass group will be called *secondary nuclei*.

1.2 Magnetic horizon

When the typical inter-source distance d_s is large (the source density $n_\mathrm{s} = 1/d_\mathrm{s}^3$ is low) low-energy particles propagating diffusively in the intergalactic magnetic field may not have enough time to reach the Earth even from the closest sources,[2] leading to a modification of the spectrum [11–13].

We consider a turbulent and isotropic intergalactic magnetic field, characterized by the root-mean-square amplitude (B_rms) and the coherence length (L_coh). A critical energy can be defined as that for which the effective Larmor radius equals the coherence length. For a particle of atomic number Z it is given by $E_\mathrm{crit} \equiv ZR_\mathrm{crit}$, with $R_\mathrm{crit} \equiv |e|B_\mathrm{rms}L_\mathrm{coh} \simeq 0.9(B_\mathrm{rms}/\mathrm{nG})(L_\mathrm{coh}/\mathrm{Mpc})$ EeV. The sources are consider to be homogeneously distributed and with a steady emission over cosmological times.

The spectrum reaching the Earth in the presence of magnetic fields can be obtained from that in the absence of magnetic fields just through a multiplicative factor, as [14, 15]

$$J(E) \equiv G(E/E_\mathrm{crit})J_{B=0}(E), \qquad G(x) = \exp\left[-\left(\frac{a\,X_\mathrm{s}}{x + b\,(x/a)^\beta}\right)^\alpha\right], \tag{2}$$

where $X_\mathrm{s} = d_\mathrm{s}/\sqrt{r_H L_\mathrm{coh}}$, with $r_H = c/H_0$ the Hubble radius. The parameters α, β, a and b depend on the evolution of the sources, on whether particles are primary or secondary nuclei, and on the spectral index of the sources [15].

The suppression factor G is plotted in Figure 1 for different X_s and for the NE and SFR scenarios. The different suppression of primary and secondary particles arises from their different average travel times. The latter have a higher average redshift of production (in photodisintegration processes) than that of primaries, resulting in longer travel times. The magnetic suppression is also milder for the SFR than for the NE scenario due to the longer average travel times associated to the former.

If one considers magnetic field amplitudes in the range $4\,\mathrm{nG} < B_\mathrm{rms} < 100\,\mathrm{nG}$ and coherence lengths such that $25\,\mathrm{kpc} < L_\mathrm{coh} < 1\,\mathrm{Mpc}$, one expects the critical rigidy to be $0.1\,\mathrm{EeV} < R_\mathrm{crit} < 100\,\mathrm{EeV}$. Moreover, if $3\,\mathrm{Mpc} < d_\mathrm{s} < 40\,\mathrm{Mpc}$, one has $0.05 < X_\mathrm{s} < 4$. We thus consider parameters R_crit and X_s within these ranges when performing the fits that include the magnetic horizon effects.

We will assume that the low-energy component arises from a population of sources with a small d_s, such that the magnetic horizon effect is negligible for this component in the energy range of interest [11]. Therefore, the EGMF will only be considered to affect the high-energy component. We also assume that the contribution of Galactic cosmic rays is negligible above the energy threshold of the analysis.

[2] On average the closest source is at distance $0.55\ d_\mathrm{s}$.

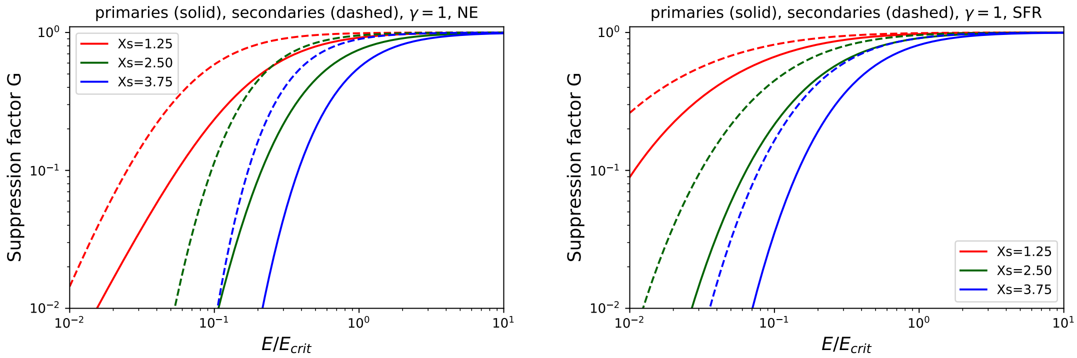

Figure 1: Magnetic suppression factor G for different values of the parameter X_s as a function of E/E_{crit}, for a spectral index of $\gamma = 1$ (suppression depends slightly on γ) for two different source evolution scenarios.

2. Combined fit to the spectrum and composition

The data sets to be fitted consist of the spectrum data from [16], for energies above $10^{17.8}$ eV and in logarithmic bins of width $\Delta \log_{10} E = 0.1$ (except at the highest energies), and the X_{max} distributions from [17], with bins of width $\Delta X_{max} = 20\,\mathrm{g\,cm^{-2}}$ in each energy interval.

We consider the functional form in Eq. (1) for the spectrum at the sources, account for the effects of interactions and redshift losses ignoring magnetic fields and then multiply the obtained fluxes by the suppression factor G in Eq. (2). We fit the parameters by maximizing a likelihood, following the procedure outlined in [1, 3]. The likelihood consists of two factors, one for the energy spectrum that is a product of Gaussian distributions for each energy bin and another for the X_{max} distributions that is a product of multinomial distributions modelled using Gumbel distribution functions, whose parameters depend on the hadronic interaction model. The likelihood $\mathcal{L}$ depends on γ_x, R^x_{cut} and element fractions $f_{A,x}$ for both components, and two extra parameters, X_s and R_{crit}, when the magnetic horizon effect is included. We report the deviance $D = -2\ln(\mathcal{L}/\mathcal{L}_{sat})$, where $\mathcal{L}$ corresponds to the model and $\mathcal{L}_{sat}$ to a model that perfectly fits the data.

EPOS-LHC

$X_s = 2.5$			NE–NE				SFR–NE					
Δ	γ_H	R^H_{cut} [EeV]	γ_L	R^L_{cut} [EeV]	R_{crit} [EeV]	D (N=353)	γ_H	R^H_{cut} [EeV]	γ_L	R^L_{cut} [EeV]	R_{crit} [EeV]	D (N=353)
1	−2.2	1.3	3.5	100	0.4	572	−2.1	1.4	3.2	100	0.0	578
2	1.0	6.2	3.6	100	3.4	586	1.1	6.2	3.3	100	3.7	588
3	1.4	7.6	3.7	100	3.3	615	1.5	7.6	3.4	100	3.5	617
no EGMF			NE–NE				SFR–NE					
1	−2.2	1.4	3.5	100	—	572	−2.1	1.4	3.2	100	—	578
2	0.2	5.8	3.6	100	—	605	0.2	5.8	3.4	100	—	607
3	0.6	7.4	3.8	100	—	651	0.6	7.4	3.5	100	—	652

Table 1: Parameters of the fit for the EPOS-LHC hadronic interactions model, different source evolution scenarios and steepness of the cutoff $\Delta = 1$, 2 or 3. The first three rows include the magnetic horizon effect (fixing $X_s = 2.5$), while the last three rows are results obtained in the absence of magnetic fields.

For simplicity we will first present results for the benchmark value of $X_s = 2.5$ so as to focus on a region of the parameters where the magnetic horizon is expected to be relevant. Table 1 presents the fit results for the EPOS-LHC model both for the case with NE in both components (NE–NE) and for the case with a SFR evolution in the low-energy component and a NE for the high-energy component (SFR–NE). A SFR evolution for the high energy component leads to worse deviances by about 35 units with respect to the corresponding NE cases, and hence we do not display them. We show the results for cutoff shapes with $\Delta = 1$, 2 or 3, including magnetic field effects and, for comparison, we also show in the last three rows those obtained in the absence of magnetic fields. The latter are consistent with the results found in [3] when a comparison can be made.

One can see that $\Delta = 1$ leads to the hardest spectrum for the high-energy sources, with $\gamma_H \simeq -2$, as well as the lowest associated cutoff rigidity, $R_{cut}^{H} \simeq 1.3$ EeV. These values are actually not independent, since to explain the pronounced flux suppression above ~ 50 EeV (which is dominated by N nuclei, implying a rigidity of ~ 7 EeV) with such a gentle cutoff and hard spectral index one needs a lower cutoff rigidity. In this case the magnetic horizon effect does not have a sizeable impact and the fit actually favours the no magnetic field case. In the case of steeper cutoffs ($\Delta = 2$ or 3), the scenarios with EGMF have smaller deviances than the cases without magnetic fields. They also lead to values of γ_H in the range from 1 to 1.5, closer to the diffusive shock acceleration (DSA) expectations and higher cutoff rigidities are obtained. We note however that the deviances for these steeper cutoff cases are higher than for the $\Delta = 1$ case.

The low-energy component has a steep spectrum (ranging from $\gamma_L = 3.3$ to 3.7, depending on the assumed evolution). This may still be consistent with the expectations from DSA if there is actually a superposition of sources with a distribution of cutoff values [18]. When considering a SFR scenario the higher luminosity present at large redshifts gives rise to stronger interactions with the CMB and EBL, resulting in a more pronounced steepening of the spectrum due to the propagation. This requires a harder input source spectrum for the low-energy component to get a similar spectrum at Earth. However, the differences in deviance and in the other fit parameters for the SFR and NE cases are quite small.

Fig. 2 displays the spectra at Earth for some illustrative cases. Dotted lines represent the flux of primary particles, while solid lines add up the flux of primary and secondary particles of each mass group at Earth. Even if the source scenarios we consider are quite different, the predicted fluxes and composition at Earth have many common features. Some of those confirm previous results, such as the dominance of heavier elements at the highest energies and that each element peaks in a narrow energy range [19]. Important contributions to the H and He components are of secondary origin, leading to a bump on the H spectrum between 3 and 10 EeV and one in the He spectrum between 5 and 20 EeV. Additionally, the majority of the low-energy component's flux consists of H and N nuclei, accompanied by a small fraction of He and negligible quantities of Si and Fe. We observe that He nuclei give rise to the instep feature of the spectrum (at ≈ 15 EeV), which arises from the source's cutoff as well as from the effects of the interactions with the CMB and EBL that cause the heavier nuclei to photo-disintegrate. Above the instep the N nuclei dominate the flux and the suppression above 50 EeV arises from a combination of the high-energy source cutoff and interactions with the CMB. Finally, Si and Fe are the main contributors to the flux at the highest energies.

We now consider the hadronic interaction model Sibyll2.3d. We present the results of the

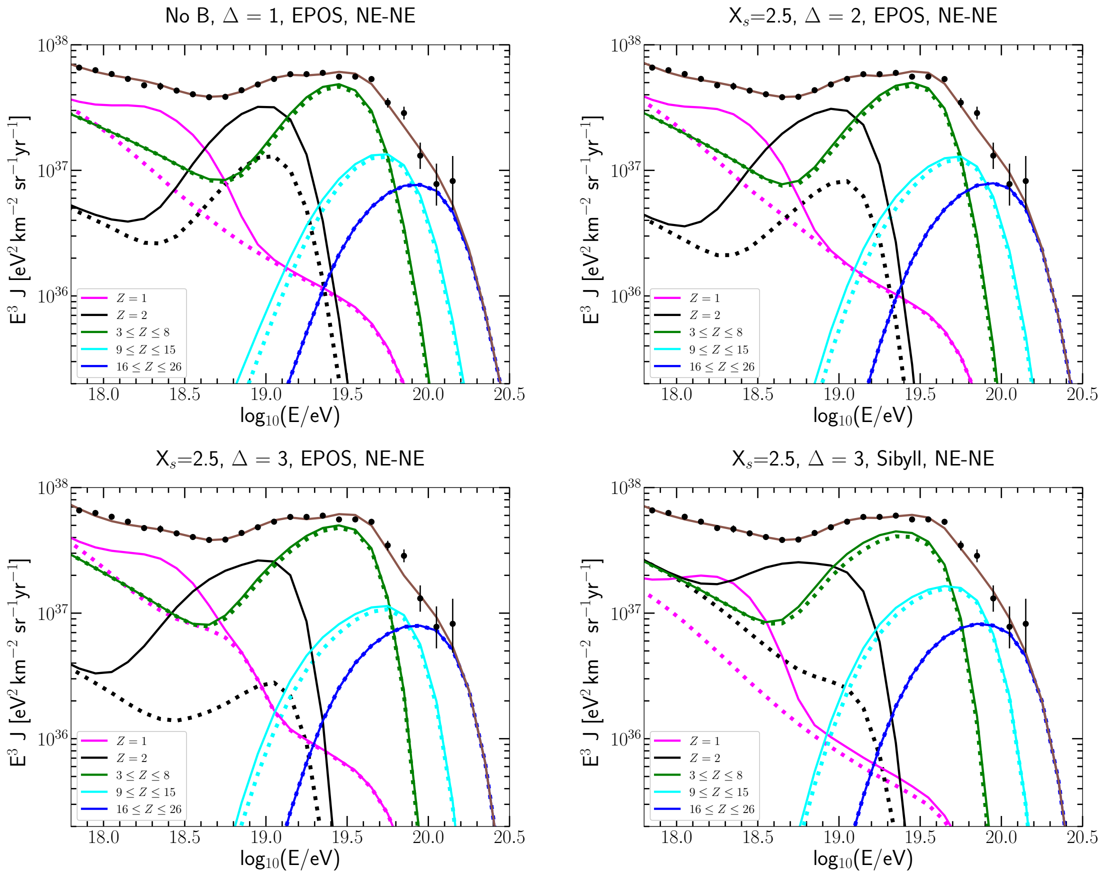

Figure 2: Fits to the flux at Earth in the NE-NE scenario. Coloured lines represent the different mass groups, while the brown one represents the total flux. Dotted lines correspond to primary nuclei, while solid lines to primaries plus secondaries. Top and bottom-left panels use EPOS-LHC hadronic model, while the bottom-right panel uses Sibyll2.3d. Top left corresponds to a case without magnetic field and $\Delta = 1$. The other three plots correspond to cases with $X_s = 2.5$. Top right has $\Delta = 2$ and bottom plots have $\Delta = 3$.

fit with this model for some representative cases on Table 2 and display the spectrum for one of them in the bottom right panel in Fig. 2. When changing from EPOS-LHC to Sibyll2.3d, the $X_{\rm max}$ predictions are shifted up and thus the fit requires a heavier composition to account for the measurements at Earth. The effect is readily seen in the low-energy component, for which the H contribution is significantly reduced, while that of He nuclei is increased (bottom panels of Fig. 2) with respecto to EPOS-LHC. One observes that for $\Delta = 1$ the smallest deviance is obtained for the $B = 0$ case, while for $\Delta = 2$ or 3 smaller deviances result when including EGMFs. For these steeper cutoff shapes the values of $\gamma_{\rm H}$ are larger, and in particular for $\Delta = 3$ the high-energy spectrum slope agrees with the expectations from DSA of $\gamma \simeq 2$. We note that the deviances obtained for Sibyll2.3d are larger than those for EPOS-LHC for all the cases considered.

In Fig. 3 we show the results of the fit obtained when we scan over the values of the parameter X_s, which up to now was kept fixed at the value 2.5. The two left plots show the best fit values of $R_{\rm crit}$ and $\gamma_{\rm H}$ obtained, together with their uncertainties, as a function of X_s, while the right plot shows the associated deviances for different hadronic models and values of Δ. We see that

Sibyll 2.3d												
$X_s = 2.5$	NE–NE						SFR–NE					
Δ	γ_H	R^H_{cut} [EeV]	γ_L	R^L_{cut} [EeV]	R_{crit} [EeV]	D (N=353)	γ_H	R^H_{cut} [EeV]	γ_L	R^L_{cut} [EeV]	R_{crit} [EeV]	D (N=353)
1	−1.7	1.4	3.4	2.2	0.0	660	−1.6	1.4	3.0	2.9	0.0	665
2	1.2	6.4	3.5	100	2.5	639	1.4	6.3	3.2	3.5	3.3	634
3	2.0	7.6	3.6	100	3.9	640	2.0	7.4	3.3	100	4.1	637
no EGMF	NE–NE						SFR–NE					
1	−1.7	1.4	3.4	2.2	—	660	−1.6	1.4	3.0	2.9	—	665
2	0.5	6.0	3.5	100	—	661	0.5	6.2	3.2	100	—	664
3	0.8	7.4	3.6	100	—	699	0.8	7.4	3.3	100	—	698

Table 2: Same as Table 1, but using the Sibyll 2.3d hadronic interaction model.

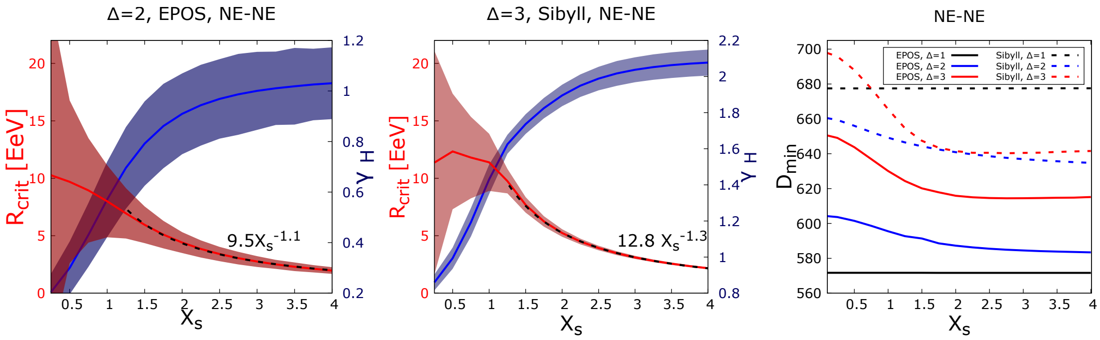

Figure 3: Best fit values of R_{crit} and γ_H as a function of X_s for the scenario with EPOS-LHC with $\Delta = 2$ (left panel) and Sibyll 2.3d with $\Delta = 3$ (middle panel), for the NE–NE scenario. Dashed lines display the behaviour of the best fit R_{crit} as function of X_s for $X_s > 1.25$. The deviance as a function of X_s is shown on the right panel for different scenarios.

the approximate relation $X_s R_{crit} \sim 10$ EeV holds when the magnetic horizon effect is relevant (for $X_s > 1.5$). Moreover, it is possible to obtain fits with very similar values of γ_H and similar deviance for these combinations of X_s and R_{crit}, as can be seen on the right plot.

It is useful to consider that these parameters are related to the inter-source separation and magnetic field characteristics through

$$\frac{X_s R_{crit}}{10\,\text{EeV}} \simeq \frac{d_s}{40\,\text{Mpc}} \frac{B_{rms}}{100\,\text{nG}} \sqrt{\frac{L_{coh}}{25\,\text{kpc}}}. \tag{3}$$

This means that a large inter-source distance, corresponding to a low density of sources, as well as a quite large *rms* amplitude of the intergalactic magnetic field within the Local Supercluster are needed in order for the magnetic horizon effect to play a relevant role in explaining the observations. These magnetic field values are in the upper range that could result for instance from the amplification of primordial seeds in the flux conserving gravitational compression during the formation of the large scale structures and the action of dynamo processes [20].

3. Conclusions

We have included in the combined fit of the spectrum and $X_{\max}$ distributions the effects of the flux suppression which appears at low rigidities when taking into account the finite CR intersource separation and the presence of extragalactic magnetic fields, what is known as the magnetic horizon effect. We explored the impact of different hadronic interaction models, cosmological source evolutions and of the steepness of the cutoff shape.

It was found that if the inter-source distances are sizeable (suggesting source densities smaller than 10^{-4} Mpc^{-3}) and if the strength of the turbulent extragalactic magnetic fields in the Local Supercluster region is large, see Eq. (3), one can obtain best fit values for the source spectral index of the high-energy population which are much closer to the expectations from diffusive shock acceleration, in contrast with the much harder source spectra inferred when the magnetic field effects are ignored. The overall features of the observed CR spectrum at the Earth are however quite similar in the different scenarios considered.

References

[1] A. Aab *et al.* [Pierre Auger Collaboration], JCAP **04** (2017) 038.
[2] E. Guido (for the Pierre Auger Collaboration), PoS(ICRC2021)311.
[3] A. Abdul Halim *et al.* [Pierre Auger Collaboration], JCAP **05** (2023) 024.
[4] M. Unger, G.R. Farrar and L. Anchordoqui, Phys. Rev. D **92** (2015) 123001.
[5] A.M. Hopkins and J.F. Beacom, Astrophys. J. **651** (2006) 142.
[6] R. Aloisio *et al.*, JCAP **11** (2017) 009.
[7] A.J. Koning, S. Hilaire and M.C. Duijvestijn, American Institute of Physics Conference Series **769** (2005) 1154.
[8] R. Gilmore, R. Somerville, J. Primack and A. Domínguez, Mon. Not. Roy. Astron. Soc. **442** (2012) 3189.
[9] T. Pierog *et al.* , Phys. Rev. C **92** (2015) 034906.
[10] F. Riehn, R. Engel, A. Fedynitch, T. K. Gaisser and T. Stanev, Phys. Rev. D **102** (2020) 063002.
[11] R. Aloisio and V. Berezinsky, Astrophys. J. **612** (2004) 900.
[12] David Wittkowski (for the Pierre Auger Collaboration), PoS(ICRC2017)563.
[13] S. Mollerach and E. Roulet, Phys. Rev. D **101** (2020) 103024.
[14] S. Mollerach and E. Roulet, JCAP **10** (2013) 013.
[15] J. González, S. Mollerach and E. Roulet, Phys. Rev. D **104** (2021) 063005.
[16] P. Abreu *et al.* [Pierre Auger Collaboration], Eur. Phys. J. C **81** (2021) 966.
[17] A. Yushkov (for the Pierre Auger Collaboration) PoS(ICRC2019)482.
[18] M. Kachelriess and D. V. Semikoz, Phys. Lett. B **634** (2006) 143.
[19] A. Aab *et al.* [Pierre Auger Collaboration], Phys. Rev. D **90** (2014) 122006.
[20] S. Hackstein, M. Brüggen, F. Vazza and L. F. S. Rodrigues, MNRAS **498** (2020) 4811.

The Pierre Auger Collaboration

P. Abreu[71], M. Aglietta[53,51], J.M. Albury[12], I. Allekotte[1], A. Almela[8,11], J. Alvarez-Muñiz[78], R. Alves Batista[79], G.A. Anastasi[62,51], L. Anchordoqui[86], B. Andrada[8], S. Andringa[71], C. Aramo[49], P.R. Araújo Ferreira[41], J. C. Arteaga Velázquez[66], H. Asorey[8], P. Assis[71], G. Avila[10], A.M. Badescu[74], A. Bakalova[31], A. Balaceanu[72], F. Barbato[44,45], R.J. Barreira Luz[71], K.H. Becker[37], J.A. Bellido[12,68], C. Berat[35], M.E. Bertaina[62,51], X. Bertou[1], P.L. Biermann[b], V. Binet[6], K. Bismark[38,8], T. Bister[41], J. Biteau[36], J. Blazek[31], C. Bleve[35], M. Boháčová[31], D. Boncioli[56,45], C. Bonifazi[25], L. Bonneau Arbeletche[20], N. Borodai[69], A.M. Botti[8], J. Brack[d], T. Bretz[41], P.G. Brichetto Orchera[8], F.L. Briechle[41], P. Buchholz[43], A. Bueno[77], S. Buitink[14], M. Buscemi[46], M. Büsken[38,8], K.S. Caballero-Mora[65], L. Caccianiga[58,48], F. Canfora[79,80], I. Caracas[37], J.M. Carceller[77], R. Caruso[57,46], A. Castellina[53,51], F. Catalani[18], G. Cataldi[47], L. Cazon[71], M. Cerda[9], J.A. Chinellato[21], J. Chudoba[31], L. Chytka[32], R.W. Clay[12], A.C. Cobos Cerutti[7], R. Colalillo[59,49], A. Coleman[92], M.R. Coluccia[47], R. Conceição[71], A. Condorelli[44,45], G. Consolati[48,54], F. Contreras[10], F. Convenga[55,47], D. Correia dos Santos[27], C.E. Covault[84], S. Dasso[5,3], K. Daumiller[40], B.R. Dawson[12], J.A. Day[12], R.M. de Almeida[27], J. de Jesús[8,40], S.J. de Jong[79,80], G. De Mauro[79,80], J.R.T. de Mello Neto[25,26], I. De Mitri[44,45], J. de Oliveira[17], D. de Oliveira Franco[21], F. de Palma[55,47], V. de Souza[19], E. De Vito[55,47], M. del Río[10], O. Deligny[33], L. Deval[40], A. di Matteo[51], C. Dobrigkeit[21], J.C. D'Olivo[67], L.M. Domingues Mendes[71], R.C. dos Anjos[24], D. dos Santos[27], M.T. Dova[4], J. Ebr[31], R. Engel[38,40], I. Epicoco[55,47], M. Erdmann[41], C.O. Escobar[a], A. Etchegoyen[8,11], H. Falcke[79,81,80], J. Farmer[91], G. Farrar[89], A.C. Fauth[21], N. Fazzini[a], F. Feldbusch[39], F. Fenu[53,51], B. Fick[88], J.M. Figueira[8], A. Filipčič[76,75], T. Fitoussi[40], T. Fodran[79], M.M. Freire[6], T. Fujii[91,e], A. Fuster[8,11], C. Galea[79], C. Galelli[58,48], B. García[7], A.L. Garcia Vegas[41], H. Gemmeke[39], F. Gesualdi[8,40], A. Gherghel-Lascu[72], P.L. Ghia[33], U. Giaccari[79], M. Giammarchi[48], J. Glombitza[41], F. Gobbi[9], F. Gollan[8], G. Golup[1], M. Gómez Berisso[1], P.F. Gómez Vitale[10], J.P. Gongora[10], J.M. González[1], N. González[13], I. Goos[1,40], D. Góra[69], A. Gorgi[53,51], M. Gottowik[37], T.D. Grubb[12], F. Guarino[59,49], G.P. Guedes[22], E. Guido[51,62], S. Hahn[40,8], P. Hamal[31], M.R. Hampel[8], P. Hansen[4], D. Harari[1], V.M. Harvey[12], A. Haungs[40], T. Hebbeker[41], D. Heck[40], G.C. Hill[12], C. Hojvat[a], J.R. Hörandel[79,80], P. Horvath[32], M. Hrabovský[32], T. Huege[40,14], A. Insolia[57,46], P.G. Isar[73], P. Janecek[31], J.A. Johnsen[85], J. Jurysek[31], A. Kääpä[37], K.H. Kampert[37], N. Karastathis[40], B. Keilhauer[40], J. Kemp[41], A. Khakurdikar[79], V.V. Kizakke Covilakam[8,40], H.O. Klages[40], M. Kleifges[39], J. Kleinfeller[9], M. Köpke[38], N. Kunka[39], B.L. Lago[16], R.G. Lang[19], N. Langner[41], M.A. Leigui de Oliveira[23], V. Lenok[40], A. Letessier-Selvon[34], I. Lhenry-Yvon[33], D. Lo Presti[57,46], L. Lopes[71], R. López[63], L. Lu[93], Q. Luce[38], J.P. Lundquist[75], A. Machado Payeras[21], G. Mancarella[55,47], D. Mandat[31], B.C. Manning[12], J. Manshanden[42], P. Mantsch[a], S. Marafico[33], A.G. Mariazzi[4], I.C. Mariş[13], G. Marsella[60,46], D. Martello[55,47], S. Martinelli[40,8], O. Martínez Bravo[63], M. Mastrodicasa[56,45], H.J. Mathes[40], J. Matthews[87], G. Matthiae[61,50], E. Mayotte[37], P.O. Mazur[a], G. Medina-Tanco[67], D. Melo[8], A. Menshikov[39], K.-D. Merenda[85], S. Michal[32], M.I. Micheletti[6], L. Miramonti[58,48], S. Mollerach[1], F. Montanet[35], C. Morello[53,51], M. Mostafá[90], A.L. Müller[8], M.A. Muller[21], K. Mulrey[14], R. Mussa[51], M. Muzio[89], W.M. Namasaka[37], A. Nasr-Esfahani[37], L. Nellen[67], M. Niculescu-Oglinzanu[72], M. Niechciol[43], D. Nitz[88], D. Nosek[30], V. Novotny[30], L. Nožka[32], A Nucita[55,47], L.A. Núñez[29], M. Palatka[31], J. Pallotta[2], P. Papenbreer[37], G. Parente[78], A. Parra[63], J. Pawlowsky[37], M. Pech[31], F. Pedreira[78], J. Pękala[69], R. Pelayo[64], J. Peña-Rodriguez[29], E.E. Pereira Martins[38,8], J. Perez Armand[20], C. Pérez Bertolli[8,40], M. Perlin[8,40], L. Perrone[55,47], S. Petrera[44,45], T. Pierog[40], M. Pimenta[71], V. Pirronello[57,46], M. Platino[8], B. Pont[79], M. Pothast[80,79], P. Privitera[91], M. Prouza[31], A. Puyleart[88], S. Querchfeld[37], J. Rautenberg[37], D. Ravignani[8], M. Reininghaus[40,8], J. Ridky[31], F. Riehn[71], M. Risse[43], V. Rizi[56,45], W. Rodrigues de Carvalho[20], J. Rodriguez Rojo[10], M.J. Roncoroni[8], S. Rossoni[42], M. Roth[40], E. Roulet[1], A.C. Rovero[5], P. Ruehl[43], S.J. Saffi[12], A. Saftoiu[72], F. Salamida[56,45], H. Salazar[63], G. Salina[50], J.D. Sanabria Gomez[29], F. Sánchez[8], E.M. Santos[20], E. Santos[31], F. Sarazin[85], R. Sarmento[71], C. Sarmiento-Cano[8],

R. Sato[10], P. Savina[55,47,33], C.M. Schäfer[40], V. Scherini[47], H. Schieler[40], M. Schimassek[38,8], M. Schimp[37], F. Schlüter[40,8], D. Schmidt[38], O. Scholten[83,14], P. Schovánek[31], F.G. Schröder[92,40], S. Schröder[37], J. Schulte[41], S.J. Sciutto[4], M. Scornavacche[8,40], A. Segreto[52,46], S. Sehgal[37], R.C. Shellard[15], G. Sigl[42], G. Silli[8,40], O. Sima[72,f], R. Šmída[91], P. Sommers[90], J.F. Soriano[86], J. Souchard[35], R. Squartini[9], M. Stadelmaier[40,8], D. Stanca[72], S. Stanič[75], J. Stasielak[69], P. Stassi[35], A. Streich[38,8], M. Suárez-Durán[13], T. Sudholz[12], T. Suomijärvi[36], A.D. Supanitsky[8], Z. Szadkowski[70], A. Tapia[28], C. Taricco[62,51], C. Timmermans[80,79], O. Tkachenko[40], P. Tobiska[31], C.J. Todero Peixoto[18], B. Tomé[71], Z. Torrès[35], A. Travaini[9], P. Travnicek[31], C. Trimarelli[56,45], M. Tueros[4], R. Ulrich[40], M. Unger[40], L. Vaclavek[32], M. Vacula[32], J.F. Valdés Galicia[67], L. Valore[59,49], E. Varela[63], A. Vásquez-Ramírez[29], D. Veberič[40], C. Ventura[26], I.D. Vergara Quispe[4], V. Verzi[50], J. Vicha[31], J. Vink[82], S. Vorobiov[75], H. Wahlberg[4], C. Watanabe[25], A.A. Watson[c], M. Weber[39], A. Weindl[40], L. Wiencke[85], H. Wilczyński[69], M. Wirtz[41], D. Wittkowski[37], B. Wundheiler[8], A. Yushkov[31], O. Zapparrata[13], E. Zas[78], D. Zavrtanik[75,76], M. Zavrtanik[76,75], and L. Zehrer[75]

———— • ————

[1] Centro Atómico Bariloche and Instituto Balseiro (CNEA-UNCuyo-CONICET), San Carlos de Bariloche, Argentina
[2] Centro de Investigaciones en Láseres y Aplicaciones, CITEDEF and CONICET, Villa Martelli, Argentina
[3] Departamento de Física and Departamento de Ciencias de la Atmósfera y los Océanos, FCEyN, Universidad de Buenos Aires and CONICET, Buenos Aires, Argentina
[4] IFLP, Universidad Nacional de La Plata and CONICET, La Plata, Argentina
[5] Instituto de Astronomía y Física del Espacio (IAFE, CONICET-UBA), Buenos Aires, Argentina
[6] Instituto de Física de Rosario (IFIR) – CONICET/U.N.R. and Facultad de Ciencias Bioquímicas y Farmacéuticas U.N.R., Rosario, Argentina
[7] Instituto de Tecnologías en Detección y Astropartículas (CNEA, CONICET, UNSAM), and Universidad Tecnológica Nacional – Facultad Regional Mendoza (CONICET/CNEA), Mendoza, Argentina
[8] Instituto de Tecnologías en Detección y Astropartículas (CNEA, CONICET, UNSAM), Buenos Aires, Argentina
[9] Observatorio Pierre Auger, Malargüe, Argentina
[10] Observatorio Pierre Auger and Comisión Nacional de Energía Atómica, Malargüe, Argentina
[11] Universidad Tecnológica Nacional – Facultad Regional Buenos Aires, Buenos Aires, Argentina
[12] University of Adelaide, Adelaide, S.A., Australia
[13] Université Libre de Bruxelles (ULB), Brussels, Belgium
[14] Vrije Universiteit Brussels, Brussels, Belgium
[15] Centro Brasileiro de Pesquisas Fisicas, Rio de Janeiro, RJ, Brazil
[16] Centro Federal de Educação Tecnológica Celso Suckow da Fonseca, Nova Friburgo, Brazil
[17] Instituto Federal de Educação, Ciência e Tecnologia do Rio de Janeiro (IFRJ), Brazil
[18] Universidade de São Paulo, Escola de Engenharia de Lorena, Lorena, SP, Brazil
[19] Universidade de São Paulo, Instituto de Física de São Carlos, São Carlos, SP, Brazil
[20] Universidade de São Paulo, Instituto de Física, São Paulo, SP, Brazil
[21] Universidade Estadual de Campinas, IFGW, Campinas, SP, Brazil
[22] Universidade Estadual de Feira de Santana, Feira de Santana, Brazil
[23] Universidade Federal do ABC, Santo André, SP, Brazil
[24] Universidade Federal do Paraná, Setor Palotina, Palotina, Brazil
[25] Universidade Federal do Rio de Janeiro, Instituto de Física, Rio de Janeiro, RJ, Brazil
[26] Universidade Federal do Rio de Janeiro (UFRJ), Observatório do Valongo, Rio de Janeiro, RJ, Brazil
[27] Universidade Federal Fluminense, EEIMVR, Volta Redonda, RJ, Brazil
[28] Universidad de Medellín, Medellín, Colombia
[29] Universidad Industrial de Santander, Bucaramanga, Colombia
[30] Charles University, Faculty of Mathematics and Physics, Institute of Particle and Nuclear Physics, Prague, Czech Republic
[31] Institute of Physics of the Czech Academy of Sciences, Prague, Czech Republic
[32] Palacky University, RCPTM, Olomouc, Czech Republic
[33] CNRS/IN2P3, IJCLab, Université Paris-Saclay, Orsay, France

[34] Laboratoire de Physique Nucléaire et de Hautes Energies (LPNHE), Sorbonne Université, Université de Paris, CNRS-IN2P3, Paris, France
[35] Univ. Grenoble Alpes, CNRS, Grenoble Institute of Engineering Univ. Grenoble Alpes, LPSC-IN2P3, 38000 Grenoble, France
[36] Université Paris-Saclay, CNRS/IN2P3, IJCLab, Orsay, France
[37] Bergische Universität Wuppertal, Department of Physics, Wuppertal, Germany
[38] Karlsruhe Institute of Technology (KIT), Institute for Experimental Particle Physics, Karlsruhe, Germany
[39] Karlsruhe Institute of Technology (KIT), Institut für Prozessdatenverarbeitung und Elektronik, Karlsruhe, Germany
[40] Karlsruhe Institute of Technology (KIT), Institute for Astroparticle Physics, Karlsruhe, Germany
[41] RWTH Aachen University, III. Physikalisches Institut A, Aachen, Germany
[42] Universität Hamburg, II. Institut für Theoretische Physik, Hamburg, Germany
[43] Universität Siegen, Department Physik – Experimentelle Teilchenphysik, Siegen, Germany
[44] Gran Sasso Science Institute, L'Aquila, Italy
[45] INFN Laboratori Nazionali del Gran Sasso, Assergi (L'Aquila), Italy
[46] INFN, Sezione di Catania, Catania, Italy
[47] INFN, Sezione di Lecce, Lecce, Italy
[48] INFN, Sezione di Milano, Milano, Italy
[49] INFN, Sezione di Napoli, Napoli, Italy
[50] INFN, Sezione di Roma "Tor Vergata", Roma, Italy
[51] INFN, Sezione di Torino, Torino, Italy
[52] Istituto di Astrofisica Spaziale e Fisica Cosmica di Palermo (INAF), Palermo, Italy
[53] Osservatorio Astrofisico di Torino (INAF), Torino, Italy
[54] Politecnico di Milano, Dipartimento di Scienze e Tecnologie Aerospaziali , Milano, Italy
[55] Università del Salento, Dipartimento di Matematica e Fisica "E. De Giorgi", Lecce, Italy
[56] Università dell'Aquila, Dipartimento di Scienze Fisiche e Chimiche, L'Aquila, Italy
[57] Università di Catania, Dipartimento di Fisica e Astronomia, Catania, Italy
[58] Università di Milano, Dipartimento di Fisica, Milano, Italy
[59] Università di Napoli "Federico II", Dipartimento di Fisica "Ettore Pancini", Napoli, Italy
[60] Università di Palermo, Dipartimento di Fisica e Chimica "E. Segrè", Palermo, Italy
[61] Università di Roma "Tor Vergata", Dipartimento di Fisica, Roma, Italy
[62] Università Torino, Dipartimento di Fisica, Torino, Italy
[63] Benemérita Universidad Autónoma de Puebla, Puebla, México
[64] Unidad Profesional Interdisciplinaria en Ingeniería y Tecnologías Avanzadas del Instituto Politécnico Nacional (UPIITA-IPN), México, D.F., México
[65] Universidad Autónoma de Chiapas, Tuxtla Gutiérrez, Chiapas, México
[66] Universidad Michoacana de San Nicolás de Hidalgo, Morelia, Michoacán, México
[67] Universidad Nacional Autónoma de México, México, D.F., México
[68] Universidad Nacional de San Agustin de Arequipa, Facultad de Ciencias Naturales y Formales, Arequipa, Peru
[69] Institute of Nuclear Physics PAN, Krakow, Poland
[70] University of Łódź, Faculty of High-Energy Astrophysics,Łódź, Poland
[71] Laboratório de Instrumentação e Física Experimental de Partículas – LIP and Instituto Superior Técnico – IST, Universidade de Lisboa – UL, Lisboa, Portugal
[72] "Horia Hulubei" National Institute for Physics and Nuclear Engineering, Bucharest-Magurele, Romania
[73] Institute of Space Science, Bucharest-Magurele, Romania
[74] University Politehnica of Bucharest, Bucharest, Romania
[75] Center for Astrophysics and Cosmology (CAC), University of Nova Gorica, Nova Gorica, Slovenia
[76] Experimental Particle Physics Department, J. Stefan Institute, Ljubljana, Slovenia
[77] Universidad de Granada and C.A.F.P.E., Granada, Spain
[78] Instituto Galego de Física de Altas Enerxías (IGFAE), Universidade de Santiago de Compostela, Santiago de Compostela, Spain
[79] IMAPP, Radboud University Nijmegen, Nijmegen, The Netherlands
[80] Nationaal Instituut voor Kernfysica en Hoge Energie Fysica (NIKHEF), Science Park, Amsterdam, The Netherlands

[81] Stichting Astronomisch Onderzoek in Nederland (ASTRON), Dwingeloo, The Netherlands
[82] Universiteit van Amsterdam, Faculty of Science, Amsterdam, The Netherlands
[83] University of Groningen, Kapteyn Astronomical Institute, Groningen, The Netherlands
[84] Case Western Reserve University, Cleveland, OH, USA
[85] Colorado School of Mines, Golden, CO, USA
[86] Department of Physics and Astronomy, Lehman College, City University of New York, Bronx, NY, USA
[87] Louisiana State University, Baton Rouge, LA, USA
[88] Michigan Technological University, Houghton, MI, USA
[89] New York University, New York, NY, USA
[90] Pennsylvania State University, University Park, PA, USA
[91] University of Chicago, Enrico Fermi Institute, Chicago, IL, USA
[92] University of Delaware, Department of Physics and Astronomy, Bartol Research Institute, Newark, DE, USA
[93] University of Wisconsin-Madison, Department of Physics and WIPAC, Madison, WI, USA

—–

[a] Fermi National Accelerator Laboratory, Fermilab, Batavia, IL, USA
[b] Max-Planck-Institut für Radioastronomie, Bonn, Germany
[c] School of Physics and Astronomy, University of Leeds, Leeds, United Kingdom
[d] Colorado State University, Fort Collins, CO, USA
[e] now at Hakubi Center for Advanced Research and Graduate School of Science, Kyoto University, Kyoto, Japan
[f] also at University of Bucharest, Physics Department, Bucharest, Romania

Acknowledgments

The successful installation, commissioning, and operation of the Pierre Auger Observatory would not have been possible without the strong commitment and effort from the technical and administrative staff in Malargüe. We are very grateful to the following agencies and organizations for financial support:

Argentina – Comisión Nacional de Energía Atómica; Agencia Nacional de Promoción Científica y Tecnológica (ANPCyT); Consejo Nacional de Investigaciones Científicas y Técnicas (CONICET); Gobierno de la Provincia de Mendoza; Municipalidad de Malargüe; NDM Holdings and Valle Las Leñas; in gratitude for their continuing cooperation over land access; Australia – the Australian Research Council; Belgium – Fonds de la Recherche Scientifique (FNRS); Research Foundation Flanders (FWO); Brazil – Conselho Nacional de Desenvolvimento Científico e Tecnológico (CNPq); Financiadora de Estudos e Projetos (FINEP); Fundação de Amparo à Pesquisa do Estado de Rio de Janeiro (FAPERJ); São Paulo Research Foundation (FAPESP) Grants No. 2019/10151-2, No. 2010/07359-6 and No. 1999/05404-3; Ministério da Ciência, Tecnologia, Inovações e Comunicações (MCTIC); Czech Republic – Grant No. MSMT CR LTT18004, LM2015038, LM2018102, CZ.02.1.01/0.0/0.0/16_013/0001402, CZ.02.1.01/0.0/0.0/18_046/0016010 and CZ.02.1.01/0.0/0.0/17_049/0008422; France – Centre de Calcul IN2P3/CNRS; Centre National de la Recherche Scientifique (CNRS); Conseil Régional Ile-de-France; Département Physique Nucléaire et Corpusculaire (PNC-IN2P3/CNRS); Département Sciences de l'Univers (SDU-INSU/CNRS); Institut Lagrange de Paris (ILP) Grant No. LABEX ANR-10-LABX-63 within the Investissements d'Avenir Programme Grant No. ANR-11-IDEX-0004-02; Germany – Bundesministerium für Bildung und Forschung (BMBF); Deutsche Forschungsgemeinschaft (DFG); Finanzministerium Baden-Württemberg; Helmholtz Alliance for Astroparticle Physics (HAP); Helmholtz-Gemeinschaft Deutscher Forschungszentren (HGF); Ministerium für Kultur und Wissenschaft des Landes Nordrhein-Westfalen; Ministerium für Wissenschaft, Forschung und Kunst des Landes Baden-Württemberg; Italy – Istituto Nazionale di Fisica Nucleare (INFN); Istituto Nazionale di Astrofisica (INAF); Ministero dell'Universitá e della Ricerca (MUR); CETEMPS Center of Excellence; Ministero degli Affari Esteri (MAE), ICSC Centro Nazionale di Ricerca in High Performance Computing, Big Data and Quantum Computing, funded by European Union NextGenerationEU, reference code CN_00000013; México – Consejo Nacional de Ciencia y Tecnología (CONACYT) No. 167733; Universidad Nacional Autónoma de México (UNAM); PAPIIT DGAPA-UNAM; The Netherlands – Ministry of Education, Culture and Science; Netherlands Organisation for Scientific Research (NWO); Dutch national e-infrastructure with the support of SURF Cooperative; Poland – Ministry of Education and Science, grants No. DIR/WK/2018/11 and 2022/WK/12; National Science Centre, grants No. 2016/22/M/ST9/00198, 2016/23/B/ST9/01635, 2020/39/B/ST9/01398, and 2022/45/B/ST9/02163; Portugal – Portuguese national funds and FEDER funds within Programa Operacional Factores de Competitividade through

Fundação para a Ciência e a Tecnologia (COMPETE); Romania – Ministry of Research, Innovation and Digitization, CNCS-UEFISCDI, contract no. 30N/2023 under Romanian National Core Program LAPLAS VII, grant no. PN 23 21 01 02 and project number PN-III-P1-1.1-TE-2021-0924/TE57/2022, within PNCDI III; Slovenia – Slovenian Research Agency, grants P1-0031, P1-0385, I0-0033, N1-0111; Spain – Ministerio de Economía, Industria y Competitividad (FPA2017-85114-P and PID2019-104676GB-C32), Xunta de Galicia (ED431C 2017/07), Junta de Andalucía (SOMM17/6104/UGR, P18-FR-4314) Feder Funds, RENATA Red Nacional Temática de Astropartículas (FPA2015-68783-REDT) and María de Maeztu Unit of Excellence (MDM-2016-0692); USA – Department of Energy, Contracts No. DE-AC02-07CH11359, No. DE-FR02-04ER41300, No. DE-FG02-99ER41107 and No. DE-SC0011689; National Science Foundation, Grant No. 0450696; The Grainger Foundation; Marie Curie-IRSES/EPLANET; European Particle Physics Latin American Network; and UNESCO.